Wang et al. *EPJ Quantum Technology* (2023) 10:34
https://doi.org/10.1140/epjqt/s40507-023-00191-0

EPJ Quantum Technology
a SpringerOpen Journal

RESEARCH Open Access

Simultaneous cooling and synchronization of the mechanical and the radio-frequency resonators via voltage modulation

Liang Wang[1], Wei Zhang[1], Shutian Liu[1*], Shou Zhang[2*] and Hong-Fu Wang[2*]

*Correspondence: stliu@hit.edu.cn; szhang@ybu.edu.cn; hfwang@ybu.edu.cn
[1]School of Physics, Harbin Institute of Technology, Harbin, Heilongjiang 150001, China
[2]Department of Physics, College of Science, Yanbian University, YanJi, JiLin 133002, China

Abstract

We explore the ground state cooling and quantum synchronization of the mechanical and low-frequency inductor-capacitor (LC) resonators in a hybrid three-mode optoelectromechanical system, in which the mechanical resonator is optically and capacitively coupled to the optical cavity and the LC circuit, respectively. We find that when the bias voltage modulation switch is incorporated into the direct current (DC) bias voltage, ground state cooling and quantum synchronization can be simultaneously achieved regardless of whether the mechanical resonator and the low-frequency LC resonator have the identical frequency. Furthermore, we elucidate the relationship between quantum synchronization and ground state cooling of the two resonators, that is, the simultaneous ground state cooling of the resonators must be accompanied by quantum synchronization. Our work may open up an alternative approach to the simultaneous ground state cooling and quantum synchronization of multiple resonators, which has fewer parametric limitations.

Keywords: Ground state cooling; Quantum synchronization; Optoelectromechanical system

1 Introduction

Over the past decades, benefiting from advancements in micro-nano manufacturing technology, a new experimental achievement has been made: the realization of macroscopic quantum states [1]. The macroscopic mechanical resonator has become an excellent tool for advancing our understanding of the quantum world. Most research on mechanical quantum states focuses on optomechanics, electromechanics, and magnomechanics [2–6], such as quantum mechanical squeezing [7–9], quantum entanglement [10–12], superposition states [13], radiation pressure interaction [14], and so on. Meanwhile, these studies are indispensable to the advancement of quantum information processing, with applications in precise measurement [15–17], quantum communication [18, 19], quantum teleportation [20, 21], nonreciprocal transmission [22–24], and quantum transducers [25, 26]. However, the observation of these phenomena in mechanical systems is not effortless due to the inevitable thermal fluctuations that disrupt a series of above quantum effects. Therefore, to observe the signature of the aforementioned quantum effects,

the primary prerequisite is to cool the mechanical resonators to their ground states effectively suppressing adverse effects of mechanical noise. For this purpose, several alternative cooling schemes have been proposed, such as backaction cooling [27, 28], laser cooling [29, 30], dissipative cooling [31], and sideband cooling [32–34].

With further research on mechanical systems and the rapid development of semiconductor technology, a number of theoretical and experimental investigations have concentrated on optomechanical and electromechanical systems, involving two or even multiple mechanical modes. Recently, the radiation pressure interaction between the cavity field and mechanical resonator has expanded beyond the conventional optical frequency domain. Studies have also been conducted on the interaction between microwave and mechanical resonators by employing LC circuits, which has gained popularity in transducing radio-frequency and microwave signals to the optical spectrum [2, 35–51]. In the standard optomechanical and electromechanical systems, observing the quantum properties requires cooling mechanical mode to its quantum ground state [52–54]. Nevertheless, to successfully establish the phonon-phonon cooling channel, a strict parametric constraint in previous studies is that the frequencies of the coupled mechanical resonators should be degenerate or nearly degenerate. Therefore, one may inquire whether an effective approach exists to simultaneously cool two non-degenerate resonators.

Huygens first observed that the oscillations of the two pendulum clocks tend to synchronize [55]. Since then, the complex and fascinating phenomenon of synchronization has attracted widespread attention, and the classical concept of synchronization was extended to continuous variable subsystems [56, 57]. In the past decades, the concept of synchronization has been proposed theoretically and realized experimentally [58–60]. Classical synchronization theory is a dynamic theory based on classical Newtonian mechanics or analytical mechanics. Quantum synchronization is a synchronization phenomenon in the field of quantum mechanics, and quantum synchronization theory is regarded as a correction of the influence of quantum fluctuations on the basis of classical synchronization theory. Unlike classical synchronization, quantum synchronization focuses on the behavior of quantum systems rather than considering classical systems. With the development of quantum mechanics, synchronization is gradually extended to the micro- and nano-scale, and quantum effects may cause some differences between classical and quantum synchronization. Due to the unique properties of quantum mechanics, such as entanglement and superposition, which do not exist in classical systems. Surprisingly, the fluctuation in the two subsystems in quantum synchronization must strictly adhere to the Heisenberg uncertainty principle [61], and extending from classical to quantum synchronization is not straightforward. In 2011, Mari *et al.* introduced the concepts of quantum synchronization and quantum phase synchronization, and proposed two different quantum synchronization measures [62]. The study of the synchronization behavior among substances in multibody physical systems has been extended from the classical to the quantum fields [63, 64]. Especially, Yang *et al.* have observed the synchronization and cooling behavior [65]. Remarkably, the simultaneous cooling of two mechanical resonators with large frequency difference and their quantum synchronization have not received considerable attention.

Sympathetic cooling of a radio-frequency LC circuit to its ground state has been first proposed in Ref. [53]. It is worth noting that what we study in this paper is only slightly similar in the model but somewhat different in the content of the study. The previous study primarily focusing on the cooling effect of the mechanical and radio-frequency resonators

at the identical frequency. Our work investigate the simultaneous ground state cooling of the mechanical and radio-frequency resonators with identical or different frequencies by injecting voltage modulation switch. Furthermore, we investigate the relationship between quantum synchronization and ground state cooling, providing a comprehensive and detailed explanation. Our work may relax experimental restrictions in practical implementations.

In this paper, we investigate ground state cooling and synchronization of the mechanical and low-frequency LC resonators in a optoelectromechanical system. We introduce a bias voltage modulation switch into LC circuit to achieve the simultaneous cooling of the non-degenerate mechanical and radio-frequency (rf) resonators. This modulation restructures a beam splitter-type interaction between the mechanical and rf resonators, improving the cooling efficiency and quantum synchronization of the two resonators. We also demonstrate the relationship between quantum synchronization and simultaneous ground state cooling, that is, cooling is a sufficient condition for synchronization. As our analysis exhibits, quantum synchronization primarily depends on the ground state cooling of the mechanical and rf resonators rather than their frequency difference. Therefore, simultaneous ground state cooling of the two resonators is a prerequisite for quantum synchronization, irrespective of the present degree of frequency difference.

2 System and Hamiltonian

We consider a hybrid optoelectromechanical system in Fig. 1, where the mechanical resonator is a silicon nitride film capable of free vibration, which has been implemented in experiments [38]. In addition, the vibration of the film modifies the resonant frequency of the optical cavity and adjusts the capacitance of the LC circuit, leading to the frequency change of the rf resonator. On the one hand, the mechanical resonator with the frequency ω_0 is capacitively coupled to a low-frequency LC circuit with the frequency $\omega_{\rm lc}$, which has been proposed and characterized in previous experiments [39, 66]. On the other hand, the mechanical resonator is coupled to a cavity field with the frequency ω_a via the radia-

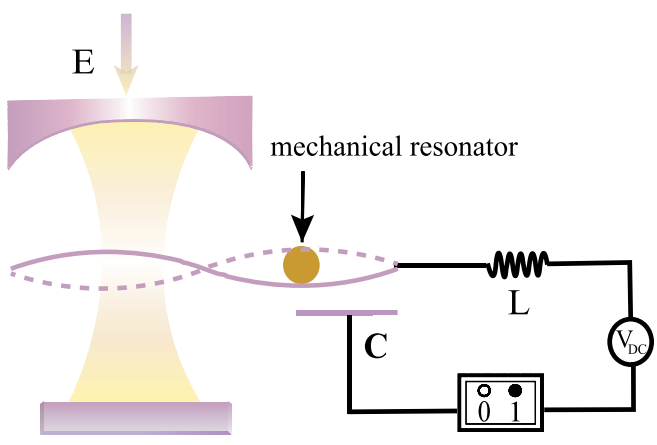

Figure 1 Schematic diagram of the system. The mechanical resonator is capacitively coupled to the LC circuit and dispersively coupled to the optical cavity via the radiation pressure. The circuit consists of a capacitor C and an inductor L. The cavity field is driven by the pump laser with the amplitude E and the LC circuit is driven by a DC bias voltage V. We introduce a voltage modulation switch $\eta = 0, 1$ in the circuit and $V = V_{\rm DC}\cos(\eta\omega t)$, where $\omega = |\omega_0 - \omega_{\rm lc}|$ is modulation frequency

tion pressure. It is worth noting that only mechanical and rf resonators with comparable frequencies are considered in the scheme. Therefore, in a rotating frame at the input laser frequency ω_l, the transformed Hamiltonian of the whole system is given by

$$H_0 = \Delta a^\dagger a + \frac{\omega_0}{2}\left(p_1^2 + q_1^2\right) + \frac{\omega_{\rm lc}}{2}\left(p_2^2 + q_2^2\right) + g_1 a^\dagger a q_1 + g_2 q_1 q_2^2 + E\left(a + a^\dagger\right) + q_2 V(t), \tag{1}$$

where $\Delta = \omega_a - \omega_l$ is cavity-driven laser detuning. a ($a^\dagger$) represents the annihilation (creation) operator of the optical mode, q_1 and p_1 (q_2 and p_2) denote the dimensionless position and momentum operators of mechanical (rf) resonator, respectively. g_1 (g_2) represents the coupling strength between the mechanical resonator and cavity field (rf resonator). $E = \sqrt{2\kappa P/\hbar\omega_l}$ is the driving strength with ω_l being the driving frequency, P the power, and κ the cavity mode decay rate. We introduce the external bias voltage $V(t) = V'(t) + \delta V(t)$, where $V'(t) = V_{\rm DC}\cos(\eta\omega t)$ represents the modulated DC bias voltage. The voltage modulation switch $\eta = 0, 1$ controls the DC bias voltage amplitude of the LC circuit, which manipulates the effective coupling between the two resonators. The input noise δV represents Johnson-Nyquist voltage noise operator [67, 68], which satisfies the correlation function: $\langle \delta V(t)\delta V(t')\rangle = \gamma_{\rm lc}(2n_{\rm lc} + 1)\delta(t - t')$. Here $n_{\rm lc} = 1/[e^{(\hbar\omega_{\rm lc}/k_B T)} - 1]$ is the mean thermal occupation number of the rf resonator, k_B is the Boltzmann constant, and T is the ambient temperature.

Quantum systems are inevitably coupled to their bath, so the motion of the system can be effectively described by the quantum Langevin equation

$$\begin{aligned}
\dot{a} &= \left(-i\Delta - \frac{\kappa}{2}\right)a - ig_1 a q_1 - E + \sqrt{\kappa}a_{\rm in},\\
\dot{p_1} &= -\omega_0 q_1 - g_1 a^\dagger a - g_2 q_2^2 - \gamma_m p_1 + \xi,\\
\dot{q_1} &= \omega_0 p_1,\\
\dot{p_2} &= -\omega_{\rm lc} q_2 - 2g_2 q_1 q_2 - \gamma_{\rm lc} p_2 - V(t),\\
\dot{q_2} &= \omega_{\rm lc} p_2,
\end{aligned} \tag{2}$$

where the mechanical and rf resonators damping rates are represented by γ_m and $\gamma_{\rm lc}$, respectively. The operators $a_{\rm in}$ and ξ represent vacuum input and Brownian motion noise operators, respectively, and in the Markovian approximation, satisfy the correlation functions $\langle a_{\rm in}(t)a_{\rm in}^\dagger(t')\rangle = \delta(t - t')$ and $\langle \xi(t)\xi(t')\rangle = \gamma_m(2n_{\rm th} + 1)\delta(t - t')$. Here, $n_{\rm th} = 1/[e^{(\hbar\omega_0/k_B T)} - 1]$ represents the equilibrium mean thermal phonon number.

Once the covariance matrix is obtained, we can study the cooling dynamics of the mechanical and rf resonators as well as the quantum synchronization (see Appendix A). The final mean phonon numbers of the mechanical and rf resonators can be expressed in terms of the matrix elements of the covariance matrix as follows

$$\begin{aligned}
n_f^1 &= \frac{1}{2}(M_{33} + M_{44} - 1),\\
n_f^2 &= \frac{1}{2}(M_{55} + M_{66} - 1).
\end{aligned} \tag{3}$$

Then the effective temperature of the mechanical and rf resonators can be obtained

$$T_{\text{eff}}^{i} = \frac{\hbar\omega_{0(\text{lc})}}{k_B \ln(1 + \frac{1}{n_f^i})} \quad (i = 1, 2). \tag{4}$$

On the other hand, the synchronization measure is a valuable tool for quantifying quantum synchronization [62], which can be defined as

$$S_c(t) = \left\langle q_-(t)^2 + p_-(t)^2 \right\rangle^{-1}, \tag{5}$$

where q_- (p_-) denotes the relative coordinates (momentum) fluctuation operator, that is $q_-(t) = [q_1(t) - q_2(t)]/\sqrt{2}$, $p_-(t) = [p_1(t) - p_2(t)]/\sqrt{2}$. In the subsequent discussion, Eq. (5) can be used to perform numerical analysis on the cooling dynamics of two resonators and investigate quantum synchronization.

3 Numerical results

3.1 The synchronization and simultaneous ground state cooling without voltage modulation ($\eta = 0$)

To ensure the rationality of the linearization process, the stability of the system should be taken into account. The system dynamics are stable when all the eigenvalues of the matrix A have negative real parts. We plot the real part of the maximum eigenvalue of the matrix A in the $P - \kappa$ plane without the voltage modulation as shown in Figs. 2(a) and 2(c). Clearly, the white dashed curve divides the system into two regions of stability and instability. As expected, the system with lower driving power P and cavity dissipation

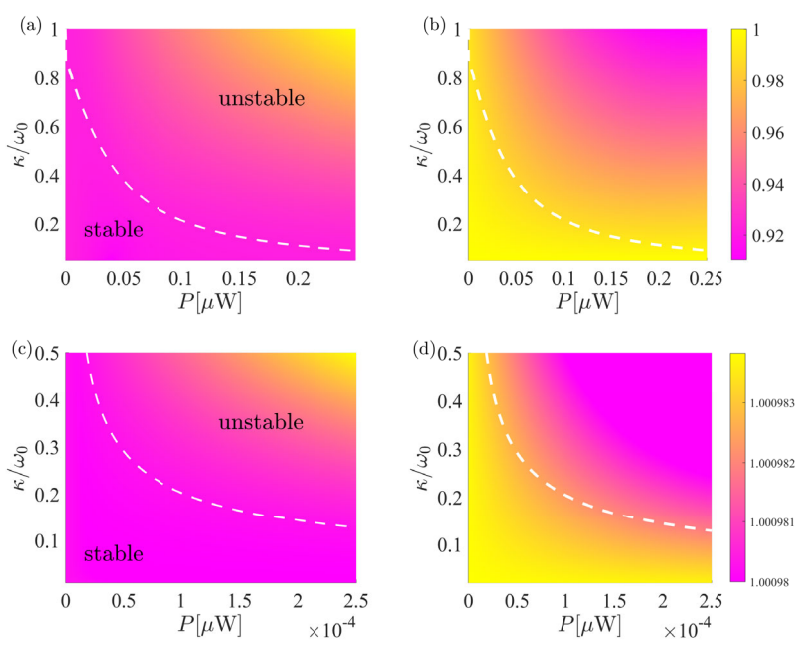

Figure 2 Phase diagram of the system stability in the P-κ plane in (a) and (c), and of the LC frequency shift $\omega'_{\text{lc}}/\omega_{\text{lc}}$ in (b) and (d) without voltage modulation ($\eta = 0$). Here we have set $\omega_0 = 2\pi \times 10^6$ Hz, $\Delta = \omega_0$, $g_1/\omega_0 = 3 \times 10^{-4}$, $g_2/\omega_0 = 5 \times 10^{-4}$, $V_{\text{DC}}/\omega_{\text{lc}} = 15$, $\gamma_m/\omega_0 = \gamma_{\text{lc}}/\omega_0 = 10^{-6}$, $T = 100$ mK, and driving field wavelength $\lambda = 1550$ nm. $\omega_{\text{lc}} = \omega_0$ in (a) and (b), $\omega_{\text{lc}}/\omega_0 = 10$ in (c) and (d)

κ is always in the stable region, no matter whether the mechanical and rf resonators have identical frequency. In the stable region, the lower driving power P can tolerate the higher dissipation κ. Moreover, in Figs. 2(b) and 2(d), we plot the effective LC frequency containing frequency shift induced by nonlinearity between the mechanical and rf resonators in the $P-\kappa$ plane. It can be observed that the LC frequency shift is derived from the nonlinear interaction between the mechanical and rf resonators, but it is almost negligible in the stability region. This means that such a frequency shift does not significantly affect the cooling dynamics of the rf resonator. Therefore, we consider $\omega'_{\rm lc} \approx \omega_{\rm lc}$ throughout the paper. In the following discussion, the selected parameters are in a stable region to ensure the system can evolve safely to a steady state.

In classical phase synchronization theory, classical synchronization is achieved when the phase difference $\phi_-(t) = \phi_1(t) - \phi_2(t)$ asymptotically converges to a constant phase [62], where $\phi_j(t) = \arctan[p_j(t)/q_j(t)]$ is jointly determined by the dimensionless position $q_j(t)$ and the momentum $p_j(t)$. In Fig. 3, we plot the time evolution of the coordinates $q_j(t)$ and the phase difference $\phi_-(t)$. Obviously, the phase difference $\phi_-(t)$ tends to be zero with the time evolution. After a long period of evolution, the coordinates $q_j(t)$ approach the identical value, indicating that classical synchronization is achieved.

To quantify the cooling performance and quantum synchronization of the mechanical and rf resonators, we plot the time evolution of the cooling dynamics and quantum synchronization for different rf resonator frequencies $\omega_{\rm lc}$ for the case without the modulation ($\eta = 0$) in Fig. 4. Note that both mechanical and rf resonators can be cooled to quantum

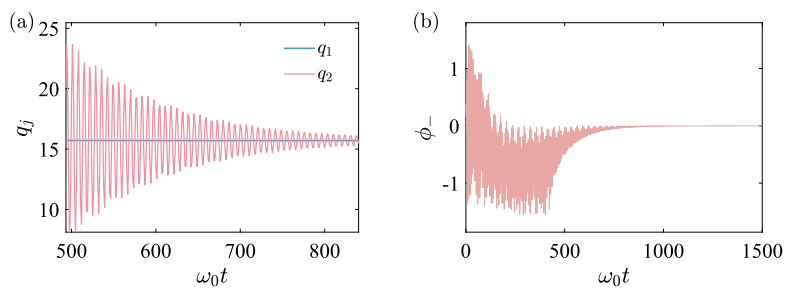

Figure 3 The time evolution of the (a) coordinates q_j and (b) phase difference ϕ_- between the mechanical and rf resonators. Here we set $\omega_{\rm lc} = \omega_0$, $\kappa/\omega_0 = 0.1$, and $P = 0.04$ μW. The other parameters are the same as in Fig. 2

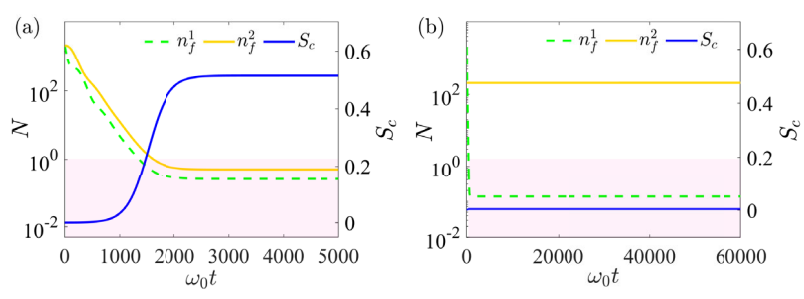

Figure 4 The time evolution of final mean phonon number n_f^i ($i = 1, 2$) and quantum synchronization S_c without the voltage modulation ($\eta = 0$). The pink shaded region signifies the ground state cooling for $N < 1$. Here we set $\omega_{\rm lc} = \omega_0$ in (a), and $\omega_{\rm lc}/\omega_0 = 10$ in (b). The other parameters are the same as in Fig. 3

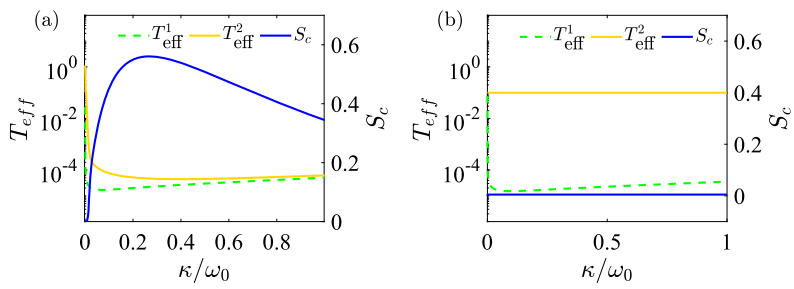

Figure 5 The effective temperature $T_{\rm eff}$ (K) and quantum synchronization S_c of mechanical and rf resonators as a function of the decay rate of cavity mode κ without the voltage modulation ($\eta = 0$). Here we set $\omega_{\rm lc} = \omega_0$ in (a), and $\omega_{\rm lc}/\omega_0 = 10$ in (b). The other parameters are the same as in Fig. 3

ground states in the steady state when two resonators possess identical eigenfrequencies ($\omega_0 = \omega_{\rm lc}$) as shown in Fig. 4(a). However, when $\omega_{\rm lc}/\omega_0 = 10$, as shown in Fig. 4(b), the steady-state mean phonon number n_f^2 is always maintained at its initial thermal occupancy. Physically, the cooling process of the mechanical resonator is the generation of anti-Stokes photons by removing a phonon from the mechanical resonator [54]. In our scheme, the mechanical resonator coupled to the cavity field is directly cooled by employing optical cold damping. On the other hand, the coupling between the mechanical and rf resonators provides an indirect channel for cooling the rf resonator due to capacitance changes, which is closely related to the effective coupling strength g. When the mechanical frequency ω_0 and the rf frequency $\omega_{\rm lc}$ are different, especially when the frequency difference is large (i.e., $|\omega_{\rm lc} - \omega_0|/G \gg 1$), the effective interaction between the mechanical and rf resonators disappears, causing the failure of ground state cooling for the rf resonator. The detailed discussions and calculations can be found in Appendix B. Moreover, it can be found that quantum synchronization is closely related to the cooling of the two resonators. A lower phonon number n_f^i corresponds to a better quantum synchronization.

In most cases, the ground state cooling and quantum synchronization are sensitive to the cavity dissipation, which determines the restrained ability of the cavity field to photons. In Fig. 5, we plot the effective temperature $T_{\rm eff}$ and quantum synchronization S_c of mechanical and rf resonators in the steady state as a function of κ/ω_0 without the voltage modulation for different rf resonator frequencies $\omega_{\rm lc}$. For Fig. 5(a), the effective temperatures of the mechanical resonator are 1×10^{-5}, 3×10^{-5}, and 6×10^{-5} K, the final mean phonon number of mechanical resonator are 0.07, 0.26 and 0.62 at $\kappa/\omega_0 = 0.1, 0.5,$ and 1, respectively. However, Fig. 5(b) shows a completely different result, where the rf resonator remains constant even when the dissipation κ is small and $\omega_{\rm lc}/\omega_0 = 10$. The corresponding mean phonon number of the rf resonator is about 207, indicating that the rf resonator cannot be cooled at all. Furthermore, the mechanical resonator is essentially unaffected by the change in the frequency of the rf resonator. Due to the significant frequency difference between the mechanical and rf resonators, the rf resonator is almost completely decoupled from the system. The cooling result of the rf resonator is only related to its bath and independent of the cavity dissipation κ. On the other hand, quantum synchronization is also sensitive to the cavity dissipation, which affects the cooling performance of both the resonators when they have identical frequencies.

In addition, the mechanical (rf) damping that indicates the coupling capability of the resonator to its bath also significantly affects the effective temperature $T_{\rm eff}$. In

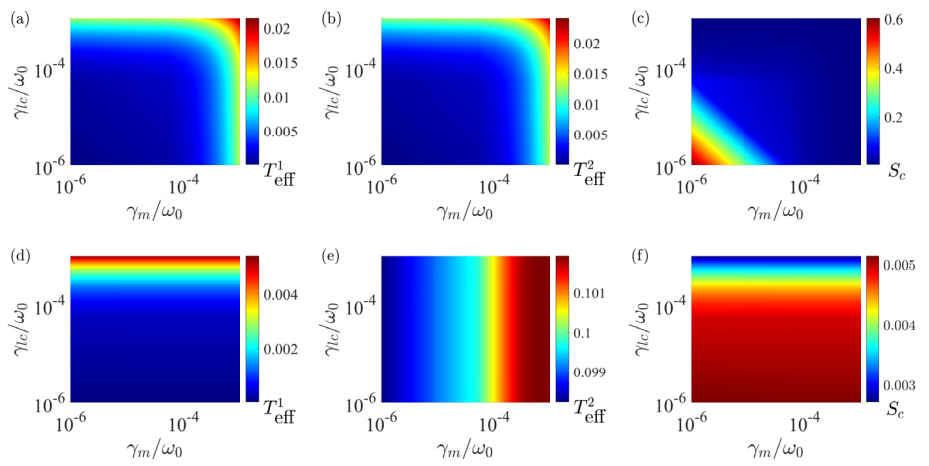

Figure 6 The effective temperature $T_{\rm eff}$ (K) and quantum synchronization S_c of mechanical and rf resonators versus γ_m and $\gamma_{\rm lc}$ without the voltage modulation ($\eta = 0$). $\omega_0 = \omega_{\rm lc}$ in (a)-(c), and $\omega_{\rm lc}/\omega_0 = 10$ in (d)-(f). The other parameters are the same as in Fig. 3

Figs. 6(a), 6(b), 6(d), and 6(e), we plot $T_{\rm eff}$ as a function of γ_m and $\gamma_{\rm lc}$ for different rf resonator frequencies $\omega_{\rm lc}$ without voltage modulation ($\eta = 0$). In Figs. 6(a) and 6(b), we can observe that when the damping rates of the mechanical resonator and the rf resonator are small, the effective temperature is lower. In Figs. 6(d) and 6(e), $\omega_{\rm lc}/\omega_0 = 10$, we can observe that changing the rf resonator frequency has little effect on the effective temperature of the mechanical resonator. However, the corresponding mean phonon number n_f^2 is about 200 at $\gamma_{\rm lc}/\omega_0 = \gamma_m/\omega_0 = 10^6$, indicating the rf resonator cannot be cooled to quantum ground state. The physical reason for this phenomenon is consistent with the above analysis, that is, the rf resonator is decoupled from the system (please see the Appendix B for details). Furthermore, quantum synchronization is closely related to the cooling results of the two resonators, as shown in Figs. 6(c) and 6(f).

In Fig. 7, we plot the final mean phonon number n_f^i and quantum synchronization S_c as a function of the photon optomechanical coupling strength g_1 and the electro-mechanical coupling rate g_2 in the steady state for different frequencies $\omega_{\rm lc}$. In Figs. 7(a) and 7(d), regardless of whether the two resonators have identical frequencies, the mechanical resonator can be cooled to the quantum ground state when single-photon optomechanical coupling strength g_1 and the electro-mechanical coupling rate g_2 are strong enough. In particular, compared to the two resonators with identical frequencies, the cooling effect of the mechanical resonator is even better when $\omega_{\rm lc}/\omega_0 = 10$. This is because the rf resonator is completely decoupled from the dynamics, so that the mechanical resonator will no longer extract the thermal excitation in the rf resonator, leading to the improvement of the net cooling efficiency. In addition, due to the dynamic decoupling of the rf resonator, the electro-mechanical coupling rate g_2 cannot affect the cooling result of the mechanical resonator, as shown in Fig. 7(d). As shown in Figs. 7(b) and 7(e), the cooling effect of the rf resonator is closely related to its frequency, which depends on its indirect interaction with the optical cold damping. At the same time, in Figs. 7(c) and 7(f), quantum synchronization also shows a trend closely related to the simultaneous ground state cooling of mechanical and rf resonators, that is, lower mean phonon numbers correspond to better quantum synchronization.

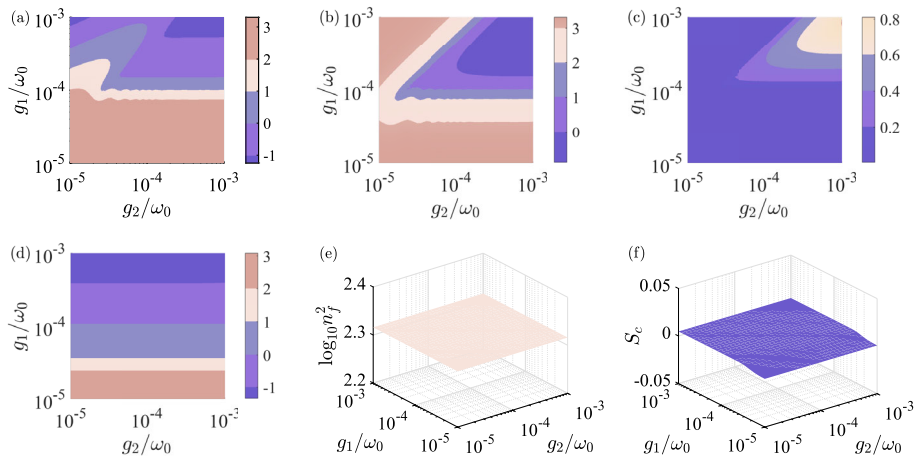

Figure 7 The final mean phonon number n_f^i and quantum synchronization S_c versus g_1 and g_2 without the voltage modulation ($\eta = 0$). $\omega_0 = \omega_{\mathrm{lc}}$ in (a)-(c), and $\omega_{\mathrm{lc}}/\omega_0 = 10$ in (d)-(f). The other parameters are the same as in Fig. 3

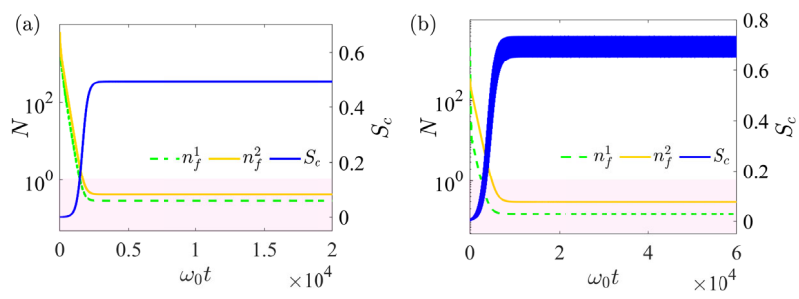

Figure 8 The time evolution of mean phonon number n_f^i and quantum synchronization S_c with the voltage modulation ($\eta = 1$). The pink shaded region signifies the ground state cooling for $N < 1$. Here we set $\omega_{\mathrm{lc}} = \omega_0$ in (a), and $\omega_{\mathrm{lc}}/\omega_0 = 10$ in (b). The other parameters are the same as in Fig. 3

3.2 The synchronization and simultaneous ground state cooling with voltage modulation ($\eta = 1$)

In the above subsection, we discussed the cooling performance and quantum synchronization of the two resonators without the voltage modulation. Especially, when the frequencies of the mechanical and rf resonators are different, the rf resonator fails to be cooled. In order to restore the cooling performance of the rf resonator in the case of large frequency difference, it is necessary to reconstruct the electro-mechanical coupling rate, which can be achieved by voltage modulation.

We plot the time evolution of cooling dynamics and quantum synchronization with the voltage modulation ($\eta = 1$) in Fig. 8. The cooling of the mechanical resonator is hardly affected compared to the case in Fig. 4(a), while the rf resonator can be successfully cooled to the quantum ground state even if the frequency difference between the two resonators is large. The reason is that the voltage modulation switch applied to the system, although the frequency of the rf resonator is much larger than the mechanical resonator ($\omega_{\mathrm{lc}}/\omega_0 = 10$), the effective beam-splitter interaction between the mechanical and rf resonators remains, leading to an indirect coupling between the rf resonator and the optical cold damping (The

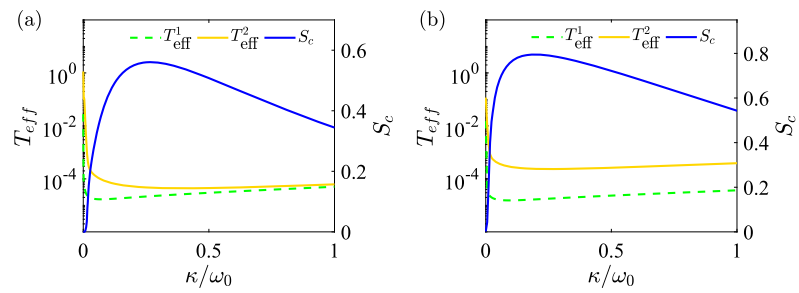

Figure 9 The effective temperature $T_{\rm eff}$ (K) and quantum synchronization S_c of mechanical and rf resonators as a function of the decay rate of cavity κ with the voltage modulation ($\eta = 1$). Here we set $\omega_{\rm lc} = \omega_0$ in (a), and $\omega_{\rm lc}/\omega_0 = 10$ in (b). The other parameters are the same as in Fig. 3

detailed discussions in the Appendix B). In addition, comparing Fig. 8(a) with Fig. 8(b), we discover that the cooling performance of the rf resonator is superior when the voltage modulation is applied to the system. The reason is that as the frequency of the rf resonator changes, its initial thermal equilibrium phonon number decreases, which allows it to eventually be cooled to a quantum state with a lower phonon number. As expected, significant quantum synchronization is also observed when the modulation is applied to the system even when $\omega_{\rm lc}/\omega_0 = 10$.

In Fig. 9, we plot the effective temperature and quantum synchronization of the mechanical and rf resonators as a function of cavity decay rate κ with the voltage modulation ($\eta = 1$). For the effective temperatures of the rf resonator are 1×10^{-5}, 2×10^{-5}, and 6×10^{-5} K, the final mean phonon number of rf resonator are 0.05, 0.15 and 0.37 at $\kappa/\omega_0 = 0.1, 0.5,$ and 1, respectively. The significant difference between Fig. 9 and Fig. 5 is that, regardless of whether the frequencies of the two resonators are identical, the rf resonator can reach quantum ground state by turning on the voltage modulation switch. It is worth noting that, the cooling properties of the cavity field are largely unaffected by the voltage modulation. The competition between the optically cold damping and the sideband conditions is still maintained, ensuring that voltage modulation can be safely applied to our scheme. In addition, even when the voltage modulation is applied to the system, quantum synchronization is still closely related to the simultaneous cooling of the two resonators.

For a complete comparison with the absence of the voltage modulation, we plot the effective temperature $T_{\rm eff}$ and quantum synchronization S_c of the two resonators as a function of $\gamma_{\rm lc}$ and γ_m with the voltage modulation ($\eta = 1$) in Fig. 10. It is obvious that the effective temperature is lower when both $\gamma_{\rm lc}$ and γ_m are small. When $\gamma_{\rm lc}/\omega_0 = \gamma_m/\omega_0 = 10^6$, the final mean phonon number of rf resonator is about 0.1. Comparing Fig. 6 with Fig. 10, in the presence of voltage modulation $\eta = 1$, and $\gamma_{\rm lc}/\omega_0 = \gamma_m/\omega_0 = 10^6$, the cooling of the rf resonator can be enhanced by a factor of about 2000 compared to that without the voltage modulation. On the other hand, this also shows that although the voltage modulation reorganizes the electro-mechanical coupling, it does not change the properties of the two resonators. In addition, we plot the final mean phonon number n_f^i as a function of g_1 and g_2 for Fig. 11. For a specific electro-mechanical coupling rate g_2, the degree of cooling improvement induced by the voltage modulation increases with the increase of the single-photon optomechanical coupling g_1, as shown in Fig. 11(e). This also confirms that the

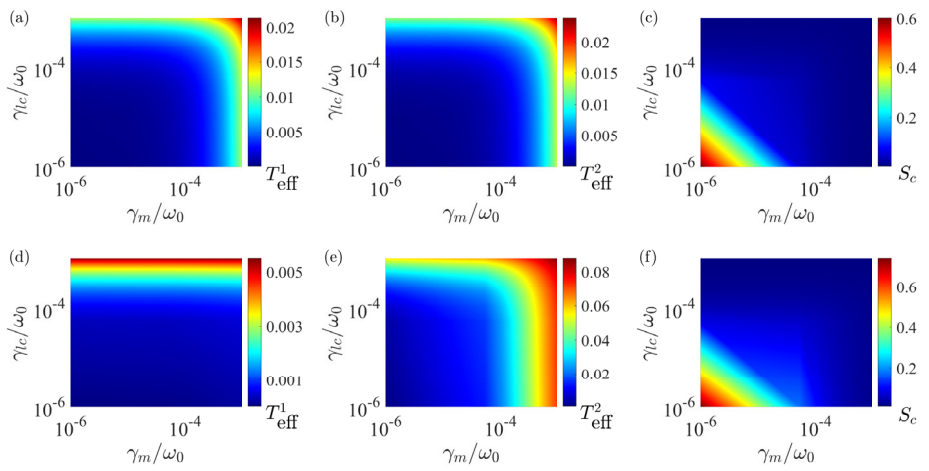

Figure 10 The effective temperature $T_{\rm eff}$ (K) and quantum synchronization S_c of mechanical and rf resonators versus γ_m and $\gamma_{\rm lc}$ with the voltage modulation ($\eta = 1$). $\omega_0 = \omega_{\rm lc}$ in (a)-(c), and $\omega_{\rm lc}/\omega_0 = 10$ in (d)-(f). The other parameters are the same as in Fig. 3

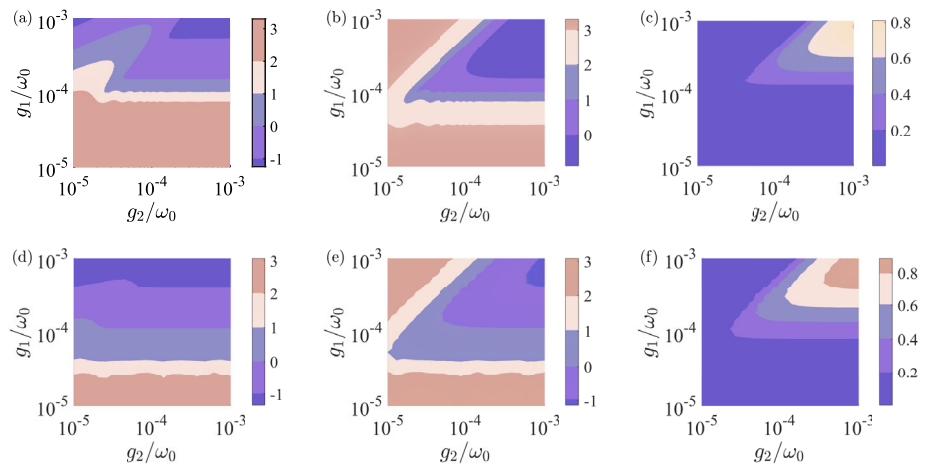

Figure 11 The final mean phonon number n_f^i and quantum synchronization S_c versus g_1 and g_2 with the voltage modulation ($\eta = 1$). $\omega_0 = \omega_{\rm lc}$ in (a)-(c), and $\omega_{\rm lc}/\omega_0 = 10$ in (d)-(f). The other parameters are the same as in Fig. 3

voltage modulation effectively improves the indirect interaction between the optical cold damping and the rf resonator.

In the previous discussion, we investigated the voltage modulation as a means of improving the temperature control of each resonator. We demonstrate that the voltage modulation can play a key role, especially when the frequencies of the resonators are mismatched. To more intuitively observe the important role of voltage modulation in the cooling dynamics of the system, we plot the final mean phonon number and quantum synchronization of the two resonators as a function of $\omega_{\rm lc}$ without (with) the modulation $\eta = 0$ ($\eta = 1$). As shown by the ginger curves in Fig. 12(a), there is only one dip located at $\omega_0 \approx \omega_{\rm lc}$ when the voltage modulation was not applied. This indicates that without voltage modulation, both ground state cooling and quantum synchronization simultaneously can be achieved

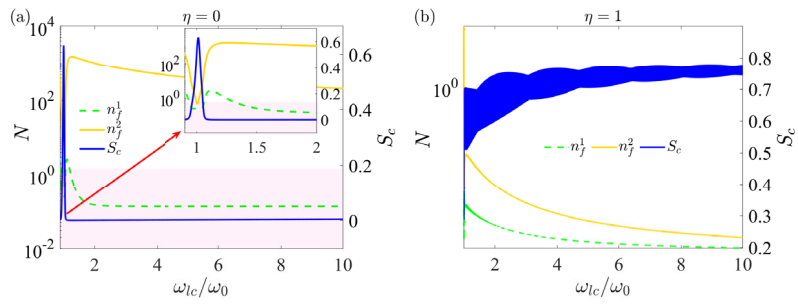

Figure 12 The final mean phonon number n_f^i and quantum synchronization S_c as a function of the frequency of the rf resonator ω_{lc} (a) without the voltage modulation ($\eta = 0$) and (b) with the voltage modulation ($\eta = 1$). The pink shaded region signifies the ground state cooling for $N < 1$. The other parameters are the same as in Fig. 3

only when the frequencies of the two resonators are resonance or near resonance. The result is consistent with the results of sideband cooling in the typical optoelectromechanical system [53]. However, as shown in Fig. 12(b), when we injected the voltage modulation, we noticed the steady-state mean phonon number n_f^2 is much lower than the case of without the modulation. This indicates that the ground state cooling dynamics is significantly improved. At the same time, the voltage modulation also restores the quantum synchronization, confirming that the quantum synchronization is closely related to the simultaneous ground state cooling. Comparing Figs. 12(a) and 12(b), we can find that introducing voltage modulation switch is an effective method to achieve simultaneous ground state cooling and quantum synchronization of two resonators, regardless of whether the frequencies between the mechanical and rf resonators are identical.

4 Discussions

In this section, we discuss the experimental feasibility of our scheme. We consider a hybrid optoelectromechanical system consisting of an optical cavity, a mechanical resonator, and an rf resonator. Similar system models have been implemented experimentally [35]. Based on the hybrid optoelectromechanical system without voltage modulation, many fascinating physical phenomena have been investigated in previous studies, such as cooling [53] and entanglement [69]. The application of hybrid quantum systems has received widespread attention, for example, in the conversion of radio frequency signals to optical frequencies [35, 39]. The ground state cooling of rf circuits can be achieved by studying the interactions in hybrid optoelectromechanical systems, usually with macro-sized circuit elements. Different types of systems and structures have been proposed and experimentally characterized [35, 38, 39, 45, 66]. In our scheme, the electromechanical coupling rate can be significantly improved by DC driving the voltage in the LC circuit. The time-dependent bias voltage modulation for mechanical resonator has been realized experimentally [70]. Since we have demonstrated, when the mechanical and rf resonator have different frequencies, both the ground state cooling and quantum synchronization can be achieved by voltage modulation. It is feasible to use the voltage modulation switch to prove the cooling result. Therefore, the cooling scheme is experimentally feasible.

In general, the condition for determining whether a mechanical resonator (rf resonator) can be cooled to the quantum ground state is determined by whether final mean phonon

number is less than 1 ($n_f < 1$). However, such a dynamic balance is not achieved immediately. The physical process can be better understood by Fig. 4(a). At the initial time ($\omega_0 t = 0$), there is no interaction between the systems, and the system is in the initial thermal equilibrium. The mechanical (rf) resonator is in thermal excitation equilibrium. After a short period of evolution ($\omega_0 t = 100$), the thermal phonon number of the two resonators will appear in the form of Rabi oscillation, and the system tends to evolve towards a steady state, although it does not reach the final steady state immediately. This is because both the interaction between the photon and the mechanical resonator, as well as the interaction between the mechanical and the rf resonators, is essentially an energy exchange between a large number of particle numbers. As a result, the interaction takes a certain amount of time to reach stability, rather than achieving stability instantly. The time to reach the steady state depends on the parameters of the system, such as the photon numbers, initial thermal phonon numbers, optomechanical coupling strength, electro-mechanical coupling strength, and so on. After a long period of evolution ($\omega_0 t = 4000$), the energy exchange between the components of the system reaches dynamic equilibrium, and the number of thermal excitation of the two resonators can be approximated as constant.

An experimentally achievable silicon nitride membrane forms the mechanical resonator [38]. The two different frequencies of the resonators considered in this scheme have also been experimentally realized [11, 64]. In this paper, we choose the frequency of the rf resonator as $\omega_{\rm lc} = 2\pi \times 10^6$ Hz. In contrast to the scheme using GHz resonators, this scheme consider the rf resonator around MHz, as the lower frequency LC resonator corresponds to a tremendous amount of charge [39, 66]. Radio frequency signals in the MHz domain are widely used in various research fields and are advantageous for sensitive astrophysics detection.

On the other hand, the synchronization phenomenon has extended to the quantum domain. Many researchers have connected quantum synchronization with quantum correlation [62, 63]. The concept of synchronization can be divided into classical synchronization and quantum synchronization. Experimentally, the synchronous measurement of the system is realized by optomechanical devices [59, 64]. Quantum synchronization is a relatively new field of research, and researchers are still facing significant challenges in areas such as quantum computing and quantum sensing. The concepts of multi-mode cooling and synchronization have been proposed, but the relationship between them needs to be clarified. The synchronization and cooling relationship between two resonators has been proposed in Ref. [65]. Therefore, it is feasible to discuss the relationship between ground state cooling and quantum synchronization of two resonators. Regarding the synchronization phenomenon, the system initially exhibits more irregular oscillations for a shorter period, and then transitions into a relatively regular and stable oscillation over time. Since $\phi_- = \phi_1 - \phi_2$, the system moves to a stable equilibrium position regardless of the initial phase difference. With time evolution, the phase difference gradually tends to zero, and the coordinates are almost identical with long time evolution, signifying classical synchronization is achieved. Based on the above discussion, our scheme is feasible experimentally.

5 Conclusions

In conclusion, we have proposed a highly effective scheme for enhancing the ground state cooling and quantum synchronization of the mechanical and rf resonators in optoelectromechanical systems. Even at ultracryogenic temperatures, we find that the rf resonator

is thermally excited due to its low frequency. We demonstrate that the two resonators can be cooled to the quantum ground states by introducing a DC bias voltage modulation switch, regardless of whether the frequencies of the two resonators are identical or largely different. When the frequencies of two resonators are identical, the rf resonator can be cooled to the quantum ground state by the beam-splitter interaction with the mechanical resonator, regardless of whether the modulation is present. However, when the voltage modulation is not introduced, the effective electro-mechanical coupling between the two resonators will disappear if the frequency difference of the two resonators is large. Once the bias gate voltage modulation switch is turned on, the beam-splitter interaction can be reconstructed, which is essential for the ground state cooling of the rf resonator. Furthermore, we find that quantum synchronization is also achieved when ground state cooling is realized, but the ground state cooling is not a necessary condition for quantum synchronization. Controlling rf circuits at the quantum level is extremely significant due to its potential for detecting the rf signals with higher sensitivity. Moreover, our work has unique advantages for manipulating rf signals of various frequencies, which may be useful in detecting diverse quantum-limited rf signals.

Appendix A: Linearization of the system Hamiltonian

Since the cavity field is in a strong driving regime, the system can be manipulated by linearized Langevin equations in order to study the mechanical and rf resonators cooling. Under the case, the operators can be expressed as a sum of steady state mean value and a small quantum fluctuation operator, i.e., $O = O_s + \delta O$ ($O = a, q_1, q_2, p_1, p_2$). The steady-state solution in Eq. (2) can be calculated as

$$\begin{aligned}
\alpha_s &= \frac{E}{i\Delta_{\text{eff}} + \kappa/2}, \\
p_{1s} &= 0, \\
q_{1s} &= -\frac{g_1|\alpha_{1s}|^2 + g_2 q_{2s}^2}{\omega_0}, \\
p_{2s} &= 0, \\
q_{2s} &= \frac{V_{\text{DC}}\cos(\eta\omega t)}{\omega_{\text{lc}} + 2G_2},
\end{aligned} \tag{6}$$

and the linear quantum Langevin equations for the quantum fluctuations

$$\begin{aligned}
\delta\dot{a} &= \left(-i\Delta_{\text{eff}} - \frac{\kappa}{2}\right)\delta a_1 - iG_1\delta q_1 + \sqrt{\kappa}a_{\text{in}}, \\
\delta\dot{p}_1 &= -\omega_0\delta q_1 - G\left(\delta a^\dagger + \delta a\right) - \gamma_m\delta p_1 - g\delta q_2 + \xi, \\
\delta\dot{q}_1 &= \omega_0\delta p_1, \\
\delta\dot{p}_2 &= -\omega'_{\text{lc}}\delta q_2 - \delta V - g\delta q_1 - \gamma_{\text{lc}}\delta p_2, \\
\delta\dot{q}_2 &= \omega_{\text{lc}}\delta p_2,
\end{aligned} \tag{7}$$

where $\Delta_{\text{eff}} = \Delta + g_1 q_{1s}$, $g = 2g_2 V_{\text{DC}} \cos(\eta\omega t)/\omega'_{\text{lc}}$, $G_1 = g_1\alpha_{1s}$, $G_2 = g_2 q_{1s}$, and $\omega'_{\text{lc}} = \omega_{\text{lc}} + 2G_2$. For convenience, we drop the fluctuation operator symbol "δ" throughout the rest of the text (i.e., $\delta a \to a$).

Due to the linearity of dynamics and input noise with a zero-mean Gaussian nature, the state of the system will maintain their Gaussian nature, which indicates that the stationary state of the system will evolve towards a Gaussian state [71]. Therefore, the properties related to the dynamics of the system are entirely characterized by a covariance matrix denoted as $M(t)$ whose matrix elements are defined as

$$M_{kl}(t) = \frac{1}{2}\langle u_k(t)u_l(t) + u_l(t)u_k(t)\rangle \quad (k, l = 1, 2, \ldots, 6), \tag{8}$$

where $u(t) = [X(t), Y(t), q_1(t), p_1(t), q_2(t), p_2(t)]^T$ is the vector of the quadrature fluctuation operators. The quadrature fluctuation operators with regard to the cavity field can be expressed as $X(t) = [a^\dagger(t) + a(t)]/\sqrt{2}$, $Y(t) = i[a^\dagger(t) - a(t)]/\sqrt{2}$, and corresponding quadrature noise operators are $X^{\text{in}}(t) = [a^\dagger_{\text{in}}(t) + a_{\text{in}}(t)]/\sqrt{2}$, $Y^{\text{in}}(t) = i[a^\dagger_{\text{in}}(t) - a_{\text{in}}(t)]/\sqrt{2}$.

The equations of motion for the system in Eq. (7) can be rewritten as

$$\dot{u}(t) = A(t)u(t) + n(t), \tag{9}$$

where $n(t) = [\sqrt{\kappa}X^{\text{in}}(t), \sqrt{\kappa}Y^{\text{in}}(t), 0, \xi(t), 0, -\delta V(t)]^T$ is the vector of noise operators and the drift matrix

$$A = \begin{bmatrix} -\frac{\kappa}{2} & \Delta & 0 & 0 & 0 & 0 \\ -\Delta & -\frac{\kappa}{2} & -\sqrt{2}G_1 & 0 & 0 & 0 \\ 0 & 0 & 0 & \omega_0 & 0 & 0 \\ -\sqrt{2}G_1 & 0 & -\omega_0 & -\gamma_m & -g & 0 \\ 0 & 0 & 0 & 0 & 0 & \omega_{\text{lc}} \\ 0 & 0 & -g & 0 & -\omega'_{\text{lc}} & -\gamma_{\text{lc}} \end{bmatrix}, \tag{10}$$

where G_1 has been assumed to be real. From Eqs. (8) and (9), we obtain the covariance matrix $M(t)$, which governs the steady state of the system by solving the Lyapunov equation [72]

$$A(t)M(t) + M(t)A^T(t) = -D, \tag{11}$$

where $D = \text{Diag}[\kappa/2, \kappa/2, 0, \gamma_m(n_m + \frac{1}{2}), 0, \gamma_{\text{lc}}(n_{\text{lc}} + \frac{1}{2})]$ represents the diffusion matrix. Since $\omega_a \gg (\omega_0, \omega_{\text{lc}})$, it is assumed that the cavity is in a vacuum state and the mechanical (rf) resonator is initially prepared in a thermal state with temperature T during the evolution of the system, so that $M(0) = \text{Diag}[1/2, 1/2, n_m + 1/2, n_m + 1/2, n_{\text{lc}} + 1/2, n_{\text{lc}} + 1/2]$.

Appendix B: Derivation of effective electro-mechanical coupling

According to Eq. (7), after implementing the linearization procedure, the resulting Hamiltonian is

$$H_{\text{eff}} = \Delta a^\dagger a + \frac{\omega_0}{2}\left(p_1^2 + q_1^2\right) + \frac{\omega_{\text{lc}}}{2}\left(p_2^2 + q_2^2\right) + g' q_1 q_2 + G_1\left(a^\dagger + a\right)q_1, \tag{12}$$

where $g' = g\cos(\eta\omega t)$. In order to illustrate the generation of effective coupling between the mechanical and rf resonators, we redefine the new operators as

$$\begin{aligned} b_1 &= \frac{ip_1 + q_1}{\sqrt{2}}, \\ b_1^\dagger &= \frac{-ip_1 + q_1}{\sqrt{2}}, \\ b_2 &= \frac{ip_2 + q_2}{\sqrt{2}}, \\ b_2^\dagger &= \frac{-ip_2 + q_2}{\sqrt{2}}, \end{aligned} \tag{13}$$

where b_1 and b_2 denote the annihilation operators of the mechanical and rf resonators, respectively. After the conversion of operators, we insert Eq. (13) into Eq. (12), the transformed Hamiltonian can be written as

$$H'_{\text{eff}} = \Delta a^\dagger a + \omega_0 b_1^\dagger b_1 + \omega_{\text{lc}} b_2^\dagger b_2 + J\left(b_1^\dagger b_2 + b_2^\dagger b_1\right) + G\left(a^\dagger + a\right)\left(b_1^\dagger + b_1\right), \tag{14}$$

where $J = g'/2$ and $G = G_1/\sqrt{2}$. To clearly analyze the effects of the bias voltage modulation, we define the following rotating transformation

$$U(t) = \exp\left[-i\left(\Delta a^\dagger a + \omega_0 b_1^\dagger b_1 + \omega_{\text{lc}} b_2^\dagger b_2\right)t\right]. \tag{15}$$

In the rotating frame with respect to $U(t)$, the transformed Hamiltonian is

$$\begin{aligned} H_{\text{int}} &= U^\dagger(t) H'_{\text{eff}} U(t) + i\frac{dU^\dagger(t)}{dt} U(t) \\ &= H_{\text{int}}^{\text{M-R}} + H_{\text{int}}^{\text{M-O}}, \end{aligned} \tag{16}$$

with

$$\begin{aligned} H_{\text{int}}^{\text{M-R}} &= J\left[e^{-i(\omega_{\text{lc}}+\omega_0)t} b_1 b_2 + e^{-i(\omega_0-\omega_{\text{lc}})t} b_1^\dagger b_2\right] + \text{H.c.}, \\ H_{\text{int}}^{\text{M-O}} &= G\left[a b_1 e^{-i(\Delta+\omega_0)t} + a b_1^\dagger e^{-i(\Delta-\omega_0)t}\right] + \text{H.c.}, \end{aligned} \tag{17}$$

where $H_{\text{int}}^{\text{M-R}}$ denotes the interaction between the mechanical resonator and the rf resonator, and $H_{\text{int}}^{\text{M-O}}$ denotes the linear coupling between the optical field and the mechanical resonator. We can find that when the system is in the red detuning regime, the beam-splitter interaction between the optical field and the mechanical resonator dominates. In contrast, the two-mode squeezing interaction is a high-frequency oscillation term that can be neglected. Thus, the interaction Hamiltonian between the mechanical resonator and the optical field can be rewritten as

$$H_{\text{int}}^{\text{M-O}} = G\left[a b_1^\dagger e^{-i(\Delta-\omega_0)t} + \text{H.c.}\right], \tag{18}$$

so the mechanical resonator can be cooled to its quantum ground state by the optical cold damping under the appropriate parameter regime. On the other hand, the type of

interaction between the mechanical and the rf resonators is closely related to the voltage modulation switch and the frequency of the rf resonator. By choosing the voltage modulation frequency as $\omega = |\omega_0 - \omega_{\rm lc}|$, the interaction between the mechanical and rf resonators can be rewritten as

$$H_{\rm int}^{\rm M\text{-}R} = g\Big[\big(e^{i(\eta+1)(\omega_{\rm lc}-\omega_0)t} + e^{i(\eta-1)(\omega_{\rm lc}-\omega_0)t}\big)b_1^\dagger b_2 + e^{i[(\eta-1)\omega_{\rm lc}-(\eta+1)\omega_0]t}b_1 b_2 + e^{-i[(\eta+1)\omega_{\rm lc}-(\eta-1)\omega_0]t}b_1 b_2\Big] + \text{H.c.}. \tag{19}$$

On the one hand, when we turn off the voltage modulation switch ($\eta = 0$), the corresponding Hamiltonian in Eq. (19) is reduced as

$$H_{\rm int}^{\rm M\text{-}R} = g\Big[e^{-i(\omega_{\rm lc}+\omega_0)t}b_1 b_2 + e^{i(\omega_{\rm lc}-\omega_0)t}b_1^\dagger b_2\Big] + \text{H.c.}. \tag{20}$$

For two resonators with identical frequencies, the interaction Hamiltonian between the mechanical and the rf resonators can be rewritten as

$$H_{\rm int}^{\rm M\text{-}R} = g\big(b_1^\dagger b_2 + \text{H.c.}\big), \tag{21}$$

where we have ignored the high frequency oscillation term. Obviously, there is a beam-splitter interaction between the two resonators, so the rf resonator can also be cooled to its quantum ground state. However, in the case of $\omega_{\rm lc} \gg \omega_0$, for example, $\omega_{\rm lc}/\omega_0 = 10$, the interaction Hamiltonian between the mechanical and the rf resonators is

$$H_{\rm int}^{\rm M\text{-}R} = g\Big[e^{-11i\omega_0 t}b_1 b_2 + e^{9i\omega_0 t}b_1^\dagger b_2\Big] + \text{H.c.}. \tag{22}$$

Both the beam-splitter interaction and the two-mode squeezing interaction are high-frequency oscillation terms, which means that the rf resonator is almost dynamically decoupled, so that the rf resonator is always in thermal equilibrium and cannot be cooled to its quantum ground state at all, even when the system reaches its steady state, as shown by the ginger curve in Fig. 4(b). Therefore, when the voltage modulation switch is turned off, the rf resonator can only be effectively cooled if the frequencies of the two resonators are identical or nearly identical.

On the other hand, when we turn on the voltage modulation switch ($\eta = 1$), the corresponding Hamiltonian in Eq. (19) is reduced as

$$H_{\rm int}^{\rm M\text{-}R} = g\Big[e^{-2i(\omega_{\rm lc}+\omega_0)t}b_1 b_2 + \big(e^{2i(\omega_{\rm lc}-\omega_0)t} + 1\big)b_1^\dagger b_2\Big] + \text{H.c.}. \tag{23}$$

For two resonators with identical frequencies, the interaction Hamiltonian between the mechanical and the rf resonators is

$$H_{\rm int}^{\rm M\text{-}R} = 2g\big(b_1^\dagger b_2 + \text{H.c.}\big). \tag{24}$$

Obviously, the beam-splitter interaction between the two resonators still exists, so the rf resonator can be cooled to its quantum ground state, as shown in Fig. 8(a). For two resonators with large frequency difference ($\omega_{\rm lc} = 10\omega_0$), Eq. (23) can be rewritten as

$$H_{\rm int}^{\rm M\text{-}R} = g\Big[e^{-22i\omega_0 t}b_1 b_2 + \big(e^{18i\omega_0 t} + 1\big)b_1^\dagger b_2 + \text{H.c.}\Big]. \tag{25}$$

Naturally, even when the frequency difference between the two resonators is large, the resonant beam-splitter interaction $g(b_1^\dagger b_2 + b_2^\dagger b_1)$ still occurs. This makes it possible to achieve the ground state cooling of the rf resonator. Therefore, the introduced bias voltage modulation reconstructs the effective coupling between the mechanical and rf resonators. This allows them to indirectly interact with the cavity field in the red sideband regime, thus achieving ground state cooling of the rf resonator regardless of whether the frequencies between the two resonators are identical.

Funding
This work is supported by the National Natural Science Foundation of China under Grants No. 12074330, No. 62071412, and No. 12074094.

Abbreviations
LC, inductor-capacitor; DC, direct current; rf, radio-frequency.

Availability of data and materials
Not applicable. For all requests relating to the paper, please contact the author.

Declarations

Ethics approval and consent to participate
Not applicable.

Competing interests
The authors declare no competing interests.

Author contributions
LW, SL, SZ, and HFW initiated the project and wrote the manuscript. LW and WZ provided expertise on the theoretical analysis. SL, SZ, and HFW supervised the project. All authors discussed the results and contributed to the final manuscript. All authors read and approved the final manuscript.

Received: 19 June 2023 Accepted: 15 August 2023 Published online: 11 September 2023

References

1. Aspelmeyer M, Kippenberg TJ, Marquardt F. Cavity optomechanics. Rev Mod Phys. 2014;86:1391.
2. Chu YW, Gröblacher S. A perspective on hybrid quantum opto- and electromechanical systems. Appl Phys Lett. 2020;117:150503.
3. Guan SY, Wang HF, Yi XX. Cooperative-effect-induced one-way steering in open cavity magnonics. npj Quantum Inf. 2020;8:102.
4. Qu K, Agarwal GS. Phonon-mediated electromagnetically induced absorption in hybrid opto-electromechanical systems. Phys Rev A. 2013;87:031802(R).
5. Ma RC et al. Multi-functional quantum router using hybrid opto-electromechanics. Laser Phys Lett. 2018;15:035201.
6. Wang L et al. Magnon blockade in a PT-symmetric-like cavity magnomechanical system. Ann Phys. 2020;532:2000028.
7. Blencowe MP, Wybourne MN. Quantum squeezing of mechanical motion for micron-sized cantilevers. Physica B. 2000;280:555.
8. Wollman EE et al. Quantum squeezing of motion in a mechanical resonator. Science. 2015;349:952.
9. Bai CH, Wang DY, Zhang S, Wang HF. Qubit-assisted squeezing of mirror motion in a dissipative cavity optomechanical system. Sci China, Phys Mech Astron. 2019;62:970311.
10. Riedinger R et al. Remote quantum entanglement between two micromechanical oscillators. Nature (London). 2018;556:473.
11. Ockeloen-Korppi CF et al. Stabilized entanglement of massive mechanical oscillators. Nature (London). 2018;556:478.
12. Corrêa C, Vidiella-Barranco A. Quantum entanglement in a four-partite hybrid system containing three macroscopic subsystems. Eur Phys J Plus. 2022;137:473.
13. Nimmrichter S, Hornberger K. Macroscopicity of mechanical quantum superposition states. Phys Rev Lett. 2013;110:160403.
14. Clark JB, Lecocq F, Simmonds RW, Aumentado J, Teufel JD. Observation of strong radiation pressure forces from squeezed light on a mechanical oscillator. Nat Phys. 2016;12:683.
15. Pratten NA. The precise measurement of the density of small samples. J Mater Sci. 1981;16:1737.
16. Childs AM, Preskill J, Renes J. Quantum information and precision measurement. J Mod Opt. 2000;47:155.
17. Wu JF et al. Progress in precise measurements of the gravitational constant. Ann Phys. 2019;531:1900013.
18. Bose S. Quantum communication through an unmodulated spin chain. Phys Rev Lett. 2003;91:207901.
19. Gisin N, Thew RN. Photon. 2007;1:165.
20. Pirandola S, Eisert J, Weedbrook C, Furusawa A, Braunstein SL. Advances in quantum teleportation. Nat Photonics. 2015;9:641.
21. Bouwmeester D et al. Experimental quantum teleportation. Nature (London). 1997;390:575.

22. Jin BY, Argyropoulos C. Self-induced passive nonreciprocal transmission by nonlinear bifacial dielectric metasurfaces. Phys Rev Appl. 2020;13:054056.
23. Assunção TF, Nascimento EM, Lyra ML. Nonreciprocal transmission through a saturable nonlinear asymmetric dimer. Phys Rev E. 2014;90:022901.
24. Liu YM, Cheng J, Wang HF, Yi XX. Nonreciprocal photon blockade in a spinning optomechanical system with nonreciprocal coupling. Opt Express. 2023;31:12847.
25. Sun CP, Wei LF, Liu YX, Nori F. Quantum transducers: integrating transmission lines and nanomechanical resonators via charge qubits. Phys Rev A. 2006;73:022318.
26. Heugel TL, Biondi M, Zilberberg O, Chitra R. Quantum transducer using a parametric driven-dissipative phase transition. Phys Rev Lett. 2019;123:173601.
27. Niguès A, Siria A, Verlot P. Dynamical backaction cooling with free electrons. Nat Commun. 2015;6:8104.
28. Wilson-Rae I, Nooshi N, Dobrindt J, Kippenberg TJ, Zwerger W. Cavity-assisted backaction cooling of mechanical resonators. New J Phys. 2008;10:095007.
29. Wineland DJ, Itano WM. Laser cooling of atoms. Phys Rev A. 1979;20:1521.
30. Shuman ES, Barry JF, DeMille D. Laser cooling of a diatomic molecule. Nature (London). 2010;467:820.
31. Liu YC, Xiao YF, Luan XS, Wong CW. Dynamic dissipative cooling of a mechanical resonator in strong coupling optomechanics. Phys Rev Lett. 2013;110:153606.
32. Teufel JD et al. Sideband cooling of micromechanical motion to the quantum ground state. Nature (London). 2011;475:359.
33. Liu YM et al. Ground-state cooling of rotating mirror in double-Laguerre-Gaussian-cavity with atomic ensemble. Opt Express. 2018;26:6143.
34. Wang DY, Bai CH, Liu ST, Zhang S, Wang HF. Optomechanical cooling beyond the quantum backaction limit with frequency modulation. Phys Rev A. 2018;98:023816.
35. Taylor JM, Sørensen AS, Marcus CM, Polzik ES. Laser cooling and optical detection of excitations in a LC electrical circuit. Phys Rev Lett. 2011;107:273601.
36. Regal CA, Lehnert KW. From cavity electromechanics to cavity optomechanics. J Phys Conf Ser. 2011;264:012025.
37. Bochmann J, Vainsencher A, Awschalom DD, Cleland AN. Nanomechanical coupling between microwave and optical photons. Nat Phys. 2013;9:712.
38. Andrews RW et al. Bidirectional and efficient conversion between microwave and optical light. Nat Phys. 2014;10:321.
39. Bagci T et al. Optical detection of radio waves through a nanomechanical transducer. Nature (London). 2014;507:81.
40. Vainsencher A, Satzinger KJ, Peairs GA, Cleland AN. Bi-directional conversion between microwave and optical frequencies in a piezoelectric optomechanical device. Appl Phys Lett. 2016;109:033107.
41. Takeda K et al. Electro-mechano-optical detection of nuclear magnetic resonance. Optica. 2017;5:152.
42. Higginbotham AP et al. Harnessing electro-optic correlations in an efficient mechanical converter. Nat Phys. 2018;14:1038.
43. Simonsen A et al. Sensitive optomechanical transduction of electric and magnetic signals to the optical domain. Opt Express. 2019;27:18561.
44. Forsch M et al. Microwave-to-optics conversion using a mechanical oscillator in its quantum ground state. Nat Phys. 2020;16:69.
45. Jiang WT et al. Efficient bidirectional piezo-optomechanical transduction between microwave and optical frequency. Nat Commun. 2020;11:1166.
46. Fink JM, Kalaee M, Norte R, Pitanti A, Painter O. Efficient microwave frequency conversion mediated by a photonics compatible silicon nitride nanobeam oscillator. Quantum Sci Technol. 2020;5:034011.
47. Han X et al. Cavity piezo-mechanics for superconducting-nanophotonic quantum interface. Nat Commun. 2020;11:3237.
48. Arnold G et al. Converting microwave and telecom photons with a silicon photonic nanomechanical interface. Nat Commun. 2020;11:4460.
49. Zhou X, Cattiaux D, Theron D, Collin E. Electric circuit model of microwave optomechanics. J Appl Phys. 2021;129:114502.
50. Sohail A, Ahmed R, Yu CS. Switchable and enhanced absorption via qubit-mechanical nonlinear interaction in a hybrid optomechanical system. Int J Theor Phys. 2021;60:739.
51. Sohail A, Ahmed R, Yu CS, Munir T. Tunable optical response of an optomechanical system with two mechanically driven resonators. Phys Scr. 2020;95:045105.
52. Liu YM, Cheng J, Wang HF, Yi XX. Simultaneous cooling of two mechanical resonators with intracavity squeezed light. Ann Phys. 2021;533:2100074.
53. Malossi N et al. Sympathetic cooling of a radio-frequency LC circuit to its ground state in an optoelectromechanical system. Phys Rev A. 2021;103:033516.
54. Lai DG, Zou F, Hou BP, Xiao YF, Liao JQ. Simultaneous cooling of coupled mechanical resonators in cavity optomechanics. Phys Rev A. 2018;98:023860.
55. Huygens C. Oeuvres complètes de Christiaan Huygens. vol. 15. Dordrecht, Netherlands: Nijhoff M; 1893. p. 243.
56. Parlitz U, Junge L, Lauterborn W, Kocarev L. Experimental observation of phase synchronization. Phys Rev E. 1996;54:2115.
57. Zheng Z, Hu G. Generalized synchronization versus phase synchronization. Phys Rev E. 2000;62:7882.
58. Weiss T, Walter S, Marquardt F. Quantum-coherent phase oscillations in synchronization. Phys Rev A. 2017;95:041802.
59. Bagheri M, Poot M, Fan L, Marquardt F, Tang HX. Photonic cavity synchronization of nanomechanical oscillators. Phys Rev Lett. 2013;111:213902.
60. Shim SB, Imboden M, Mohanty P. Synchronized oscillation in coupled nanomechanical oscillators. Science. 2007;316;95.
61. Manzano G, Galve F, Giorgi GL, Hernández-García E, Zambrini R. Synchronization, quantum correlations and entanglement in oscillator networks. Sci Rep. 2013;3:1439.
62. Mari A, Farace A, Didier N, Giovannetti V, Fazio R. Measures of quantum synchronization in continuous variable systems. Phys Rev Lett. 2013;111:103605.

63. Bemani F, Motazedifard A, Roknizadeh R, Naderi MH, Vitali D. Synchronization dynamics of two nanomechanical membranes within a Fabry-Perot cavity. Phys Rev A. 2017;96:023805.
64. Zhang M et al. Synchronization of micromechanical oscillators using light. Phys Rev Lett. 2012;109:233906.
65. Yang Z et al. The simultaneous ground-state cooling and synchronization of two mechanical oscillators by driving nonlinear medium. Ann Phys. 2022;534:2100494.
66. Moaddel Haghighi I, Malossi N, Natali R, Di Giuseppe G, Vitali D. Multimode opto-electro-mechanical transducer for non-reciprocal conversion of radio-frequency and optical signals. Phys Rev Appl. 2018;9:034031.
67. Nyquist H. Thermal agitation of electric charge in conductors. Phys Rev. 1928;32:110.
68. Gardiner CW, Zoller P. Quantum noise. Berlin: Springer; 2004.
69. Li J, Gröblacher S. Stationary quantum entanglement between a massive mechanical membrane and a low frequency LC circuit. New J Phys. 2022;22:063041.
70. Hensinger WK et al. Ion trap transducers for quantum electromechanical oscillators. Phys Rev A. 2005;72:041405.
71. Vitali D et al. Optomechanical entanglement between a movable mirror and a cavity field. Phys Rev Lett. 2007;98:030405.
72. Parks PC, Hahn V. Stability theory. New York: Prentice Hall; 1993.

Publisher's Note